ACS OMEGA

Open Access

This article is licensed under CC-BY-NC-ND 4.0

http://pubs.acs.org/journal/acsodf

Article

Molecular Insights into Water−Chloride and Water−Water Interactions in the Supramolecular Architecture of Aconine Hydrochloride Dihydrate

Han-Qing Li,* Jia-Yin Xu, Shan-Shan Wu, and Liang Jin

Cite This: *ACS Omega* 2024, 9, 11925−11941

Read Online

ACCESS | Metrics & More | Article Recommendations | Supporting Information

ABSTRACT: Despite the previous preparation of aconine hydrochloride monohydrate (AHM), accurate determination of the crystal's composition was hindered by severely disordered water molecules within the crystal. In this study, we successfully prepared a new dihydrate form of the aconine hydrochloride [$C_{25}H_{42}NO_9^+Cl^-\cdot 2(H_2O)$, aconine hydrochloride dihydrate (AHD)] and accurately refined all water molecules within the AHD crystal. Our objective is to elucidate both water−chloride and water−water interactions in the AHD crystal. The crystal structure of AHD was determined at 136 K using X-ray diffraction and a multipolar atom model was constructed by transferring charge-density parameters to explore the topological features of key short contacts. By comparing the crystal structures of dihydrate and monohydrate forms, we have observed that both AHD and AHM exhibit identical aconine cations, except for variations in the number of water molecules present. In the AHD crystal, chloride anions and water molecules serve as pivotal connecting hubs to establish three-dimensional hydrogen bonding networks and one-dimensional hydrogen bonding chain; both water−chloride and water−water interactions assemble supramolecular architectures. The crystal packing of AHD exhibits a complete reversal in the stacking order compared to AHM, thereby emphasizing distinct disparities between them. Hirshfeld surface analysis reveals that H···Cl^- and H···O contacts play a significant role in constructing the hydrogen bonding network and chain within these supramolecular architectures. Furthermore, topological analysis and electrostatic interaction energy confirm that both water−chloride and water−water interactions stabilize supramolecular architectures through electrostatic attraction facilitated by H···Cl^- and H···O contacts. Importantly, these findings are strongly supported by the existing literature evidence. Consequently, navigating these water−chloride and water−water interactions is imperative for ensuring storage and safe processing of this pharmaceutical compound.

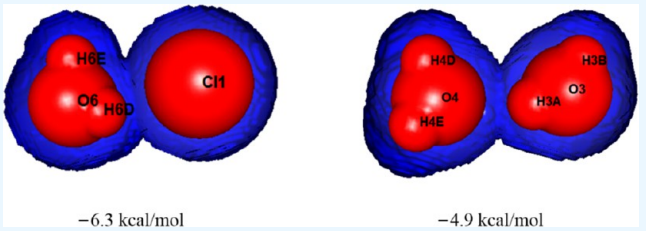

1. INTRODUCTION

The crystalline forms of an active pharmaceutical ingredient (API), including salts, hydrates, and hydrated salts, offer numerous advantages over the marketed pharmaceutical product. These advantages include impurity rejection, improved processing conditions, enhanced aqueous solubility, and greater stability.[1,2] The solid-state properties possess the potential to impact the penetrability, bioavailability, shelf life, and bioactivity of pharmaceutical products, thus significantly influencing their safety, efficacy, and quality.[3] Among various salt forms investigated, hydrochloride (HCl) salts have been extensively utilized in the pharmaceutical industry due to their low toxicity, high biocompatibility, and ability to preserve the inherent pharmacological properties of drugs.[4] The hydrous HCl salts, in which several water molecules are incorporated into their crystal lattices, represent the hydrated form of these counterparts. It is evident that hydrated HCl salts exhibit higher aqueous dissolution rate compared to their anhydrous counterparts;[2] however, under normal conditions, anhydrous forms are thermodynamically more stable than hydrates.[5]

In the supramolecular architecture[6] of hydrated HCl salt crystals, the chloride anion occupies a prominent position due to its distinctive characteristics as the sole spherical anion found in aqueous solutions and most common organic solvents. It serves as a Lewis base capable of participating in diverse supramolecular interactions with various Lewis acids.[7] However, in crystalline form, the chloride anion has been extensively utilized as a hydrogen bond acceptor in the field of supramolecular assembly[8] and as a halogen bond acceptor in domains of crystal engineering and supramolecular chemistry.[9] In hydrogen bonding, the chloride anion acts as a Lewis base by participating in H···Cl^- contacts, whereas in halogen bonding, the σ-holes[10] on the covalently bonded Br and I atoms function as Lewis acids to bind with the Lewis base such

Received: December 4, 2023
Revised: January 23, 2024
Accepted: February 14, 2024
Published: February 29, 2024

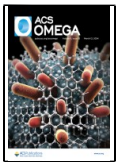

ACS Publications

© 2024 The Authors. Published by American Chemical Society

Table 1. Experimental Details for AHD and AHM Crystals[a]

	AHM (previous study)	AHD (present study)		
Crystal Data				
chemical formula	$C_{25}H_{42}NO_9^+Cl^-·H_2O$	$C_{25}H_{42}NO_9^+Cl^-·2(H_2O)$		
M_r	554.06	572.08		
crystal system, space group	orthorhombic, $P2_12_12_1$	orthorhombic, $P2_12_12_1$		
temperature (K)	293	136		
a, b, c (Å)	16.3296 (2), 16.3759 (4), 31.1186 (5)	16.3000 (8), 16.4145 (9), 31.2168 (19)		
V (Å^3)	8321.5 (3)	8352.3 (8)		
Z	12	12		
radiation type	Mo Kα	Mo Kα		
μ (mm^{-1})	0.19	0.20		
crystal size (mm)	0.35 × 0.3 × 0.25	0.35 × 0.3 × 0.25		
Data Collection				
diffractometer	Xcalibur, Eos Multiscan			
absorption correction	*CrysAlis PRO* 1.171.38.43 (Rigaku Oxford Diffraction, 2015) empirical absorption correction using spherical harmonics, implemented in SCALE3 ABSPACK scaling algorithm			
T_{min}, T_{max}	0.798, 1.000	0.454, 1.000		
no. of measured, independent, and observed [$I > 2\sigma(I)$] reflections	38668, 16991, 14265	27862, 15243, 10279		
R_{int}	0.020	0.041		
$\sin(\theta/\lambda)_{max}$ (Å^{-1})	0.625	0.625		
refinement	SHELX	SHELX_IAM	MoPro_IAM	MoPro_ELMAM2
$R[F^2 > 2\sigma(F^2)]$, $wR(F^2)$, S	0.043, 0.103, 1.03	0.048, 0.108, 0.92	0.049, 0.100, 1.06	0.039, 0.077, 0.84
no. of reflections	16991	15243	10279	10279
no. of parameters	1080	1078	1027	1483
H atom treatment	H atoms treated by a mixture of independent and constrained refinement			
$\Delta\rho_{max}$, $\Delta\rho_{min}$ (e Å^{-3})	0.65, −0.54	0.49, −0.40	0.43, −0.40	0.34, −0.32
absolute structure	Flack x determined using 5283 quotients [(I+)-(I−)]/[(I+)+(I−)] (Parsons, Flack and Wagner, Acta Cryst. B69 (2013) 249−259).			
absolute structure parameter	0.003 (15)	0.08 (3)		
CCDC	1920259	2296449	2296450	2296364

[a]Computer programs: CrysAlis PRO 1.171.38.43,[25] SHELXS,[27] SHELXL,[24] MoPro[28], Olex2.[26]

as Cl anion, forming Br···Cl$^-$ and I···Cl$^-$ contacts.[6] Indeed, halogen bonding bears resemblance to the hydrogen bonding regarding its rational manipulation of molecular recognition in the fields of chemistry and biology.[11]

The presence of water molecule in hydrated HCl salts plays a pivotal role in supporting its three-dimensional crystal structure by serving as hydrogen atom donors and participating in hydrogen bonding.[2] The distinctive characteristics of water molecule, including its relatively small size, high polarity, and ability to form hydrogen bonding network, make it indispensable building materials in the field of crystal engineering.[12] Hydrogen bonding interactions involving water molecule can be classified into three groups: water−chloride,[13] water−water,[14] and water−host.[15] Among these interactions, the water−chloride and water−water interactions are particularly significant in the crystal engineering since they greatly contribute to the overall supramolecular assembly or aggregate in hydrated HCl salts.[5]

The interaction between water and chloride is of great significance in biological environments, as well as in seawater and various geological/atmospheric processes.[13] However, in the crystal structure, the water−chloride interaction plays a crucial role in the nucleation and growth of molecular crystals, effectively modifying the physicochemical properties of APIs.[14] Additionally, calculated interaction energies for $H_2O···Cl^-$ clusters confirm that the water−chloride interaction is primarily the electrostatic attraction.[16] Meanwhile, the crucial role of water molecules in water−water interactions lies in their ability to form hydrogen bonds with other molecules and themselves; however, these hydrogen bonds do not always stabilize the crystal structure. Extensive investigations into numerous crystal structures have been conducted to probe into water−water interactions, revealing that approximately 72% of interactions between water molecules are attractive[17] while the remaining 28% exhibit repulsive interactions.[17] It is evident that favorable water−water interactions significantly stabilize the crystal structure and vice versa. Coincidentally, both water−chloride and water−water interactions typically coexist in crystalline forms of the hydrated HCl salts, forming a hydrogen-bonded cluster of water and chloride anion.[14] Regarding their effects on host molecules in the solid forms of hydrated HCl salts, it can be observed that the presence of water displaces the chloride anions from the cations and induces conformational changes in cations.[18]

Aconine, a C19-aminoalcohol diterpenoid alkaloid,[19] is present in WuTou injection.[20] It is derived from the degradation of highly toxic aconitine, a C19-diester diterpenoid alkaloid found in *Aconiti kusnezoffii radix* (known as CaoWu in Chinese).[21] The chemical structure of aconine comprises six rings, including a piperidine ring with a tertiary nitrogen atom. These six rings constitute the rigid three-dimensional central framework of aconine adorned with five alcoholic hydroxyl groups and four methoxy groups. In our previous study,[22] salt formation has been demonstrated as an

https://doi.org/10.1021/acsomega.3c09696
ACS Omega 2024, 9, 11925−11941

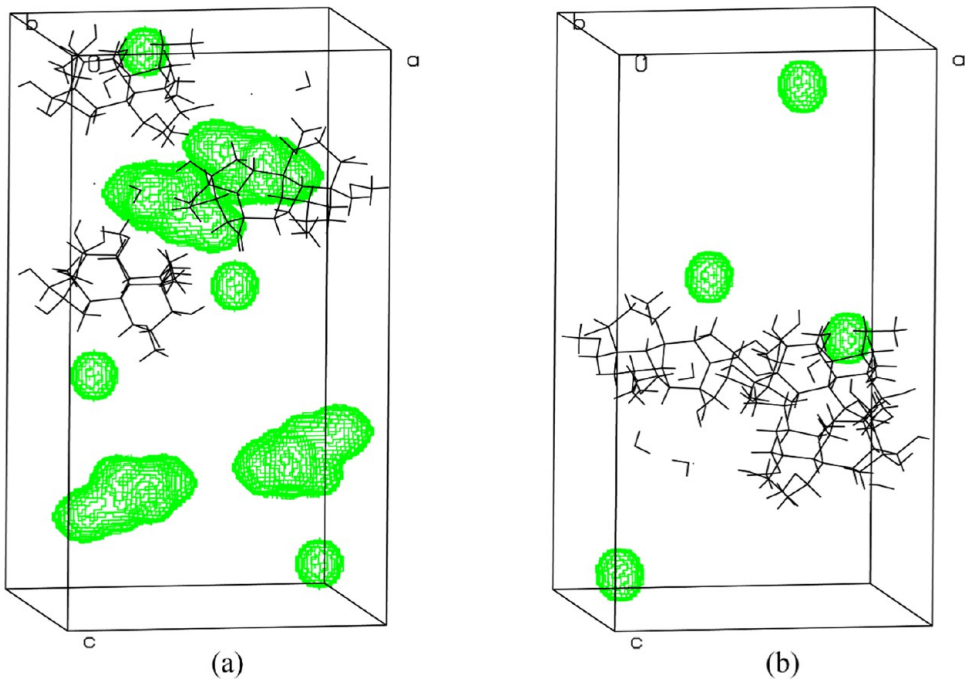

Figure 1. PLATON Solv Plots show the differences of the recovered electron density in the unit cells between AHM (a) and AHD (b). The large green spheres represent solvent voids in the unit cell of the AHM.

effective approach to modify the physicochemical properties of aconine. As a result, we have prepared one solid form of aconine hydrochloride monohydrate (AHM) in our laboratory, which effectively eliminates impurities such as residual aconitine and yellow plant pigments during the crystallization process. However, accurate determination of the crystal's composition poses challenges due to the presence of severely disordered waters in the AHM crystal.[22]

In this study, we investigate the solid-state landscape of aconine hydrochloride dihydrate (AHD), which represents a new crystalline form of aconine hydrochloride incorporating six water molecules within its asymmetric unit. The complete crystal structure was determined at 136 K using single-crystal X-ray diffraction and refined with SHELXL-IAM, MoPro-IAM, and MoPro-ELMAM2 methods. We compare the experimental findings of AHD with previous investigations on AHM. Specifically, the MoPro-ELMAM2 model is employed to explore the topological values at (3, −1) bond critical points (BCPs) in the AHD crystal, achieving multipolar modeling of low-resolution single-crystal X-ray diffraction data. Simultaneously, the modeled electron density is used to calculate electrostatic energies for both water−chloride and water−water interactions. Consequently, we provide a more comprehensive understanding of the solid-state form (dihydrate) of this pharmaceutical compound at the molecular level.

2. EXPERIMENTAL SECTION

2.1. General Materials and Methods. All analytical-grade general reagents were obtained from Sinopharm Chemical Reagent Co., Ltd. (Beijing, China). Acetonitrile of HPLC grade was purchased from Fisher Fine Chemicals Co., Ltd. (Beijing, China). Deionized water in the entire study was purified on a Milli-Q system (Millipore).

2.2. Aconine Hydrochloride Monohydrate (AHM). AHM single crystals were prepared by the previously reported method.[22] The severely disordered water molecules are embedded within the AHM crystals, hindering the refinement of the final structure and affecting the exact molecular weight. Therefore, new crystals are prepared with different solvents.

2.3. Aconine Hydrochloride Dihydrate (AHD). Appropriately 100 mg of AHM was dissolved in 20 mL of anhydrous ethanol and added with 60 mL of acetonitrile to crystallization. The resulting solution was then allowed to concentrate at room temperature until most of the solvent evaporated, yielding AHD single crystals suitable for X-ray diffraction data collection.

2.4. X-ray Crystallography. Single-crystal diffraction for AHD was performed on an Xcalibur Eos X-ray four-circle diffractometer[23] using Mo Kα radiation (0.71073 Å) with a graphite monochromator. X-ray data were collected at 136 K, avoiding solid-state transformation under a high temperature. The program ShelXL-2015[24] was used for the integration of the reflections. The structure was solved by using ShelXS[27] and refined by full-matrix least-squares technique using the ShelXL-2015.[24] The crystallographic data and structural refinement parameters are summarized in Table 1.

2.5. SHELXL-IAM Refinement. Isotropic displacement parameters are used for H atoms, and anisotropic displacement parameters are used for heavy atoms. Carbon-bound hydrogen atoms were constrained with C−H = 0.96 Å for CH_3 [Uiso(H) = 1.5Ueq(C)], C−H = 0.97 Å for CH_2 [Uiso(H) = 1.2Ueq(C)] and C−H = 0.98 Å for CH [Uiso(H) = 1.2Ueq(C)]. Amino-bound hydrogen atoms were constrained with N···H = 0.98 Å [Uiso(H) = 1.2Ueq(N)]. Oxygen-bound hydrogen atoms were constrained with O−H = 0.82 Å [Uiso(H) = 1.5Ueq(O)] or 0.85 Å [Uiso(H) = 1.5Ueq(O)] (water molecules), except for O2*A*, O2*B*, O2*C*, O5*B*, O8*B* atoms, which their O−H bonds were independently refined with different bond lengths. At the end of the SHELXL refinement, the crystallographic *R*-factor was 0.047, the weight *R*-factor was 0.105, and the goodness of fit was 0.92. The

https://doi.org/10.1021/acsomega.3c09696
ACS Omega 2024, 9, 11925−11941

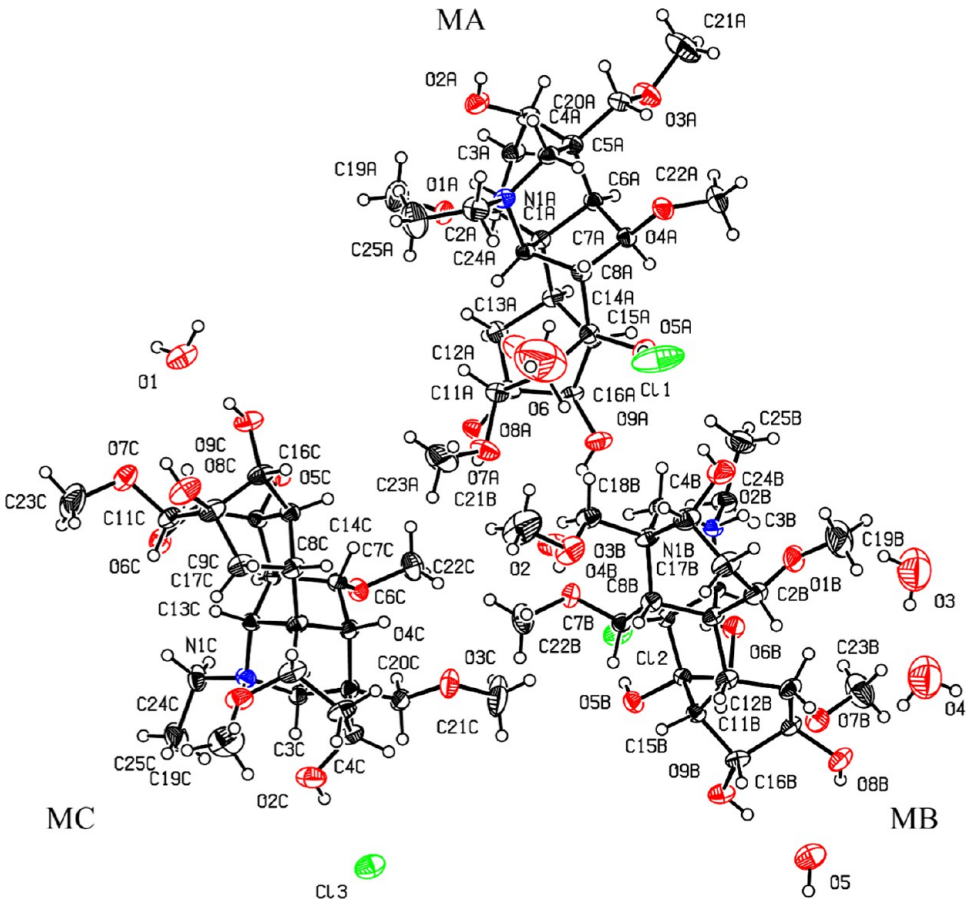

Figure 2. ORTEP-style plots for the asymmetric unit of AHD. Displacement ellipsoids are drawn at the 40% probability level. Red, blue, and green ellipsoids represent the O and N atoms and Cl anions.

Table 2. Selected Geometric Parameters (deg) for Three Aconine Cations in the AHD Crystal[a]

MA		MB		MC	
C17A−N1A−C18A−C5A	54.5(8)	C17B−N1B−C18B−C5B	50.3(8)	C17C−N1C−C18C−C5C	49.3(8)
C17A−N1A−C24A−C25A	−86.8(8)	C17B−N1B−C24B−C25B	−161.6(6)	C17C−N1C−C24C−C25C	−155.7(6)
C18A−N1A−C17A−C1A	−64.8(8)	C18B−N1B−C17B−C1B	−62.6(8)	C18C−N1C−C17C−C1C	−60.5(8)
C18A−N1A−C17A−C8A	48.1(8)	C18B−N1B−C17B−C8B	50.5(8)	C18C−N1C−C17C−C8C	52.5(8)
C18A−N1A−C24A−C25A	145.5(7)	C18B−N1B−C24B−C25B	72.8(8)	C18C−N1C−C24C−C25C	78.8(8)
C24A−N1A−C17A−C1A	167.4(6)	C24B−N1B−C17B−C1B	171.6(6)	C24C−N1C−C17C−C1C	174.7(6)
C24A−N1A−C17A−C8A	−79.8(8)	C24B−N1B−C17B−C8B	−75.3(7)	C24C−N1C−C17C−C8C	−72.4(7)
C24A−N1A−C18A−C5A	−176.9(6)	C24B−N1B−C18B−C5B	175.0(6)	C24C−N1C−C18C−C5C	174.1(5)

[a]MA, MB, and MC are three aconine cations.

maximum and minimum electron density peaks were 0.36 and −0.32 e Å^{-3}, respectively.

2.6. MoPro-IAM Refinement. The CIF of SHELXL refinement was imported into MoPro software (version 1805).[28] To make the goodness of fit close to unity, the model was built with a SHELXL-type weighting scheme of $w = 1/[2(Fo^2) + (0.0516P)^2]$, where $P = (Fo^2 + 2Fc^2)/3$. First, only the scale factor was refined until the model converged. Second, the position and displacement parameters of all nonhydrogen atoms were refined until the model converged. At the end of the MoPro-IAM refinement, the crystallographic *R*-factor was 0.049, the weight *R*-factor was 0.098, and the goodness of fit was 1.06. The maximum and minimum electron density peaks were 0.43 and −0.38 e Å^{-3}, respectively.

2.7. MoPro-ELMAM2 Refinement. The electron density multipole parameters of the Hansen & Coppens multipolar pseudoatom model[29] were transferred from the ELMAM2 library[30] using the built-in options of the MoPro software.[28] The entire asymmetric unit is electrically neutralized after the transfer with a net charge of zero. First, the scale factor, position, and displacement parameters of all nonhydrogen atoms were refined. Second, valence and dipole populations were refined. Compared with the MoPro-IAM refinement, the MoPro-ELMAM2 refinement has a great improvement over several parameters. The crystallographic *R*-factor was 0.039, the weight *R*-factor was 0.076, and the goodness of fit was 0.84. The maximum and minimum electron density peaks were 0.34 and −0.32 e Å^{-3}, respectively.

3. RESULTS AND DISCUSSION

3.1. Crystal Structure. We conducted a comparative analysis of the crystal structures of AHM and AHD,

https://doi.org/10.1021/acsomega.3c09696
ACS Omega 2024, 9, 11925−11941

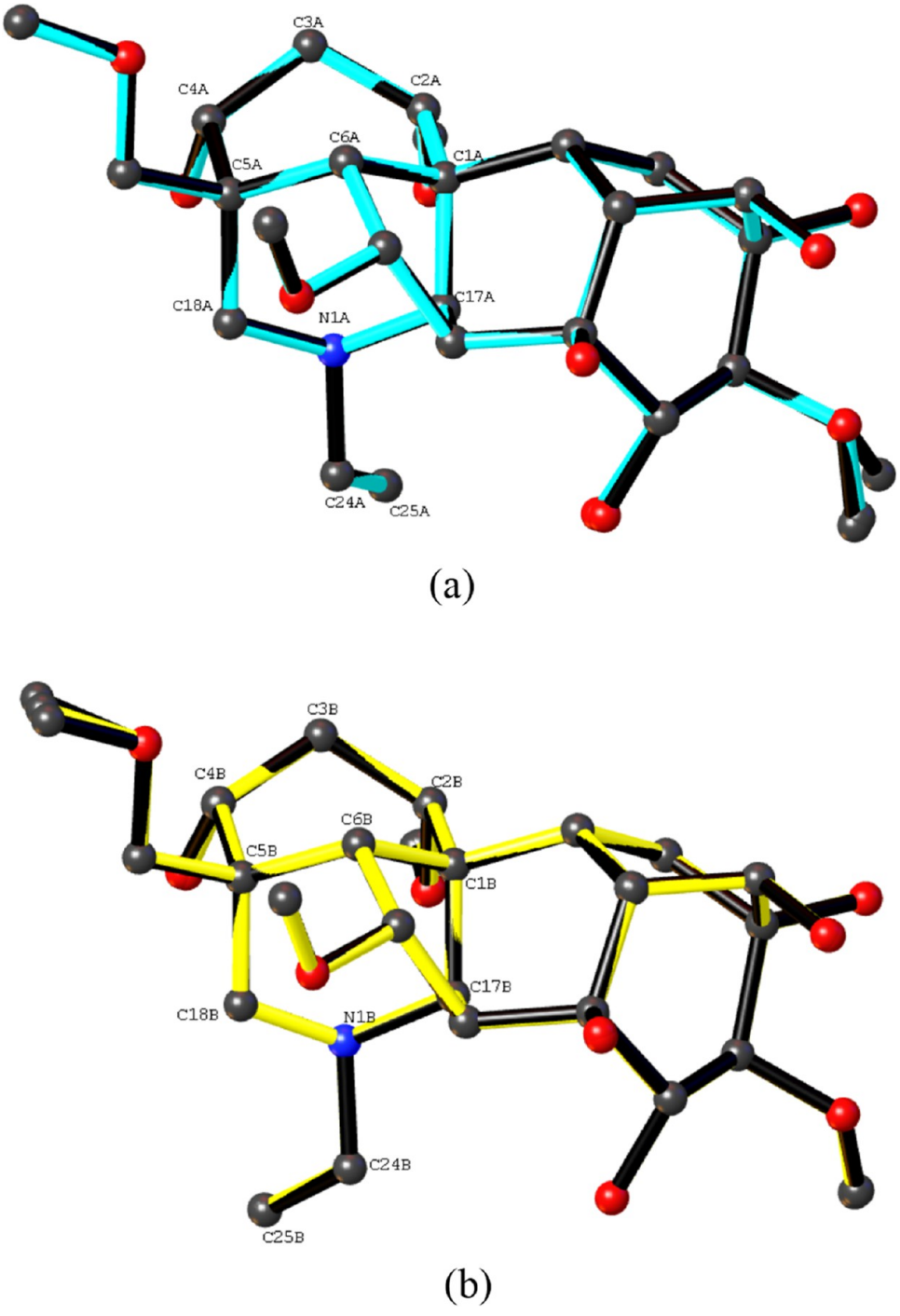

Figure 3. Overlap diagram depicting the conformational differences in the central framework between aconine cations in AHD and aconine cations in AHM: (a) MA versus M1 and (b) MB versus M2. Color codes: cyan = MA; yellow = MB; black = M1 or M2. H atoms have been omitted for clarity.

determined at different temperature conditions using X-ray diffraction. Our findings indicate that the latter exhibits higher accuracy in terms of the residual electron density peak heights (Table 1). The unit cells of the AHM and AHD are depicted in Figure 1. In the AHM crystal (Figure 1a), four prominent solvent cavities with recovered electron density are observed, while seriously disordered water molecules are eventually removed during the refinement process using PLATON.[31] Conversely, the AHD crystal (Figure 1b) does not exhibit any significant solvent cavities as all solvent molecules have been accurately refined with ideal displacement factors. Evidently, variations in the crystallographic parameters[32] confirm the discrepancies between the crystals of AHM and AHD.

The proton transfer, similar to that in the AHM crystal, induces protonation of the tertiary nitrogen atom in free aconine, leading to the ionization of each molecule (as depicted in Figure S1) within the AHD crystal. The asymmetric unit of AHD (as shown in Figure 2) comprises three aconine cations, three Cl anions, and six water molecules in a stoichiometric ratio of 1:1:2; MA (Figure S1a), MB

https://doi.org/10.1021/acsomega.3c09696
ACS Omega 2024, 9, 11925−11941

Table 3. Hydrogen Bond Geometries (Å, °) for AHD[a]

donor−hydrogen···acceptor	don−hyd	hyd−acc	don···acc	don−hyd···acc
O1−H1*D*···Cl3^{i}	0.87	2.38	3.241 (14)	173
O3−H3*B*···O9*B*^{i}	0.72	2.25	2.81 (2)	135 (2)
O2*A*−H2*A*···Cl2^{i}	0.98	2.20	3.179 (9)	174
O5*C*−H5*C*···Cl3^{ii}	0.98	2.26	3.230 (9)	168
O6*C*−H6*C*···Cl3^{ii}	0.98	2.22	3.182 (10)	166
O1−H1*E*···O4*C*^{ii}	0.83	2.03	2.84 (2)	165
O1−H1*E*···C22*C*^{ii}	0.83	2.73	3.537 (18)	164
C4*A*−H4*A*···O8*A*^{iii}	1.10	2.37	3.294 (12)	141
O6*B*−H6*B*···Cl2	0.98	2.21	3.169 (9)	165
O5*A*−H5*A*···Cl1	0.98	2.22	3.184 (10)	170
O9*A*−H9*A*···O2	0.98	1.83	2.801 (15)	170
O9*B*−H9*B*···O5	0.98	1.78	2.756 (15)	171
O8*A*−H8*A*···O2	0.98	2.63	3.308 (15)	127
O9*C*−H9*C*···O1	0.98	1.80	2.775 (16)	174
N1*A*−H1*A*···O1*A*	1.04	1.98 (2)	2.761 (18)	130
N1*A*−H1*A*···O2*A*	1.04	2.13	2.858 (13)	125
O2−H2*D*···O4*B*	0.86	2.00	2.838 (19)	163
O2−H2*E*···Cl2	0.86	2.50	3.330 (12)	161
O6*A*−H6*A*···O6	0.98	1.79 (2)	2.63 (2)	142
O8*C*−H8*C*···O1	0.98	2.47	3.240 (17)	135
N1*B*−H1*B*···O1*B*	1.04	1.92 (2)	2.69 (2)	129
N1*C*−H1*C*···O1*C*	1.04	1.86 (2)	2.620 (18)	127
O4−H4*E*···O8*B*	0.81	2.01	2.815 (19)	172
O4−H4*E*···C12*B*	0.81	2.75	3.423 (17)	142
C20*A*−H20*F*···O4*A*	1.09	2.26	2.973 (14)	121
C20*A*−H20*F*···C22*A*	1.09	2.56	3.323 (12)	126
C17*C*−H17*C*···C11*C*	1.10	2.59	3.466 (9)	136
C18*B*−H18*A*···O4*B*	1.09	2.33 (2)	3.050 (16)	122
C18*B*−H18*A*···O9*A*	1.09	2.51	3.184 (13)	119
C17*B*−H17*B*···C11*B*	1.10	2.53	3.410 (8)	136
C17*A*−H17*A*···C11*A*	1.10	2.60	3.456 (9)	134
C13*B*−H13*A*···O1*B*	1.09	2.45 (2)	3.231 (17)	128
C18*A*−H18*E*···O4*A*	1.09	2.27	3.005 (15)	123
C18*C*−H18*C*···O4*C*	1.09	2.28	2.999 (14)	121
C20*B*−H20*B*···O4*B*	1.09	2.26	2.951 (15)	119
C20*B*−H20*B*···C22*B*	1.09	2.57	3.285 (12)	122
C13*A*−H13*E*···O1*A*	1.09	2.44	3.211 (14)	127
C20*C*−H20*D*···O4*C*	1.09	2.27	2.962 (14)	119
C20*C*−H20*D*···C22*C*	1.09	2.64	3.353 (11)	122
C24*A*−H24*F*···O6*A*	1.09	2.59	3.493 (14)	139
C13*C*−H13*C*···O1*C*	1.09	2.53	3.323 (16)	128
C22*A*−H22*G*···O3*A*	1.08	2.61 (2)	3.506 (19)	140
C22*C*−H22*E*···O3*C*	1.08	2.56 (2)	3.38 (2)	133
C22*B*−H22*B*···O3*B*	1.08	2.51 (2)	3.39 (2)	139
C25*B*−H25*C*···O5*A*	1.08	2.46	3.521 (11)	169
C21*C*−H21*F*···O5*B*	1.08	2.46	3.341 (14)	139
O6−H6*D*···Cl1	0.80	2.37	2.87 (2)	122 (2)
O6−H6*E*···O3	0.93	2.19 (2)	3.03 (3)	150
O2*C*−H2*C*···Cl3	0.98	2.20	3.172 (10)	172
O8*B*−H8*B*···O5	0.98	2.13	3.011 (16)	149
O2*B*−H2*B*···Cl1	0.98	2.23	3.190 (11)	168
O5*B*−H5*B*···Cl2	0.98	2.25	3.215 (9)	168
C18*C*−H18*C*···O9*C*^{iv}	1.09	2.55	3.297 (13)	125
C18*C*−H18*D*···O5*C*^{iv}	1.09	2.47	3.474 (10)	153
C24*C*−H24*C*···O9*C*^{iv}	1.09	2.62	3.481 (14)	135
C25*C*−H25*F*···O5*C*^{iv}	1.08	2.30	3.374 (12)	177
O3−H3*A*···O4^{v}	0.82	2.06 (2)	2.81 (3)	151
C21*B*−H21*C*···O5*A*^{v}	1.08	2.57	3.574 (16)	155
O5−H5*D*···Cl1^{vi}	0.90	2.36	3.240 (13)	168
O5−H5*E*···O4*A*^{vi}	0.84	2.02	2.842 (19)	165
C19*B*−H19*A*···O6*A*^{vii}	1.08	2.47	3.413 (18)	146

https://doi.org/10.1021/acsomega.3c09696
ACS Omega 2024, 9, 11925−11941

Table 3. continued

donor−hydrogen···acceptor	don−hyd	hyd−acc	don···acc	don−hyd···acc
C19*B*−H19*B*···C25*A*[vii]	1.08	2.76	3.565 (17)	132
O4−H4*D*···O5*B*[viii]	0.84	2.06	2.885 (17)	169

[a]Symmetry codes: (i) $x-1, y, z$; (ii) $x-1/2, -y+1/2, -z+1$; (iii) $x-1/2, -y+3/2, -z+1$; (iv) $x+1/2, -y+1/2, -z+1$; (v) $-x+1, y-1/2, -z+3/2$; (vi) $x+1, y, z$; (vii) $-x+1, y+1/2, -z+3/2$; (viii) $-x+2, y+1/2, -z+3/2$.

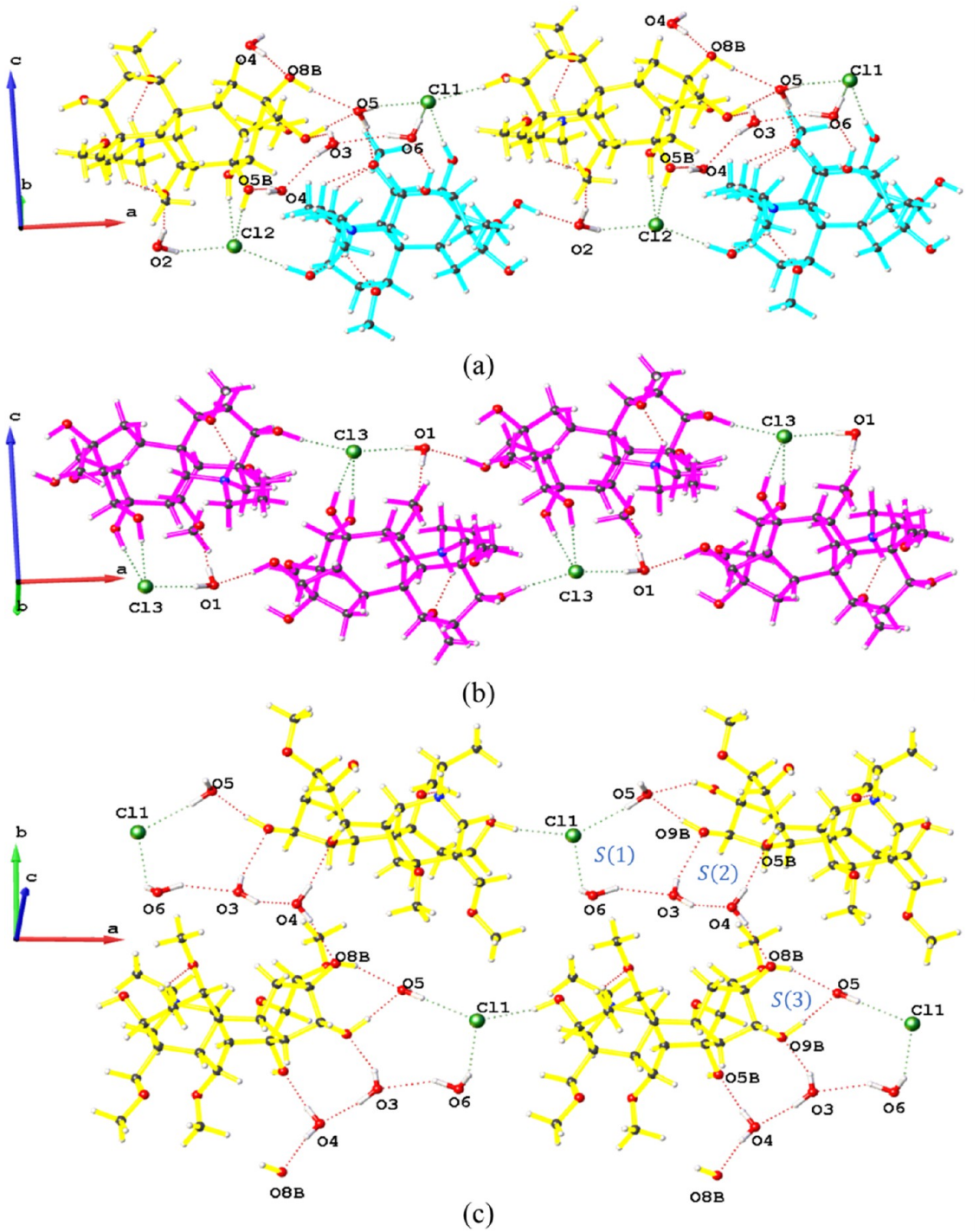

Figure 4. Supramolecular architectures with the key hydrogen bonds occurring in the AHD crystal. (a) Supramolecular architecture for AHD built from O−H···O and O−H···Cl^- hydrogen bonds (dotted lines) between MA and MB. (b) Supramolecular architecture for AHD built from the O−H···O and the O−H···Cl^- hydrogen bonds (dotted lines) among MC. (c) Water chains for AHD built from the O−H···O and O−H···Cl^- hydrogen bonds (dotted lines) among MB. For symmetry codes, see Table 3.

https://doi.org/10.1021/acsomega.3c09696
ACS Omega 2024, 9, 11925−11941

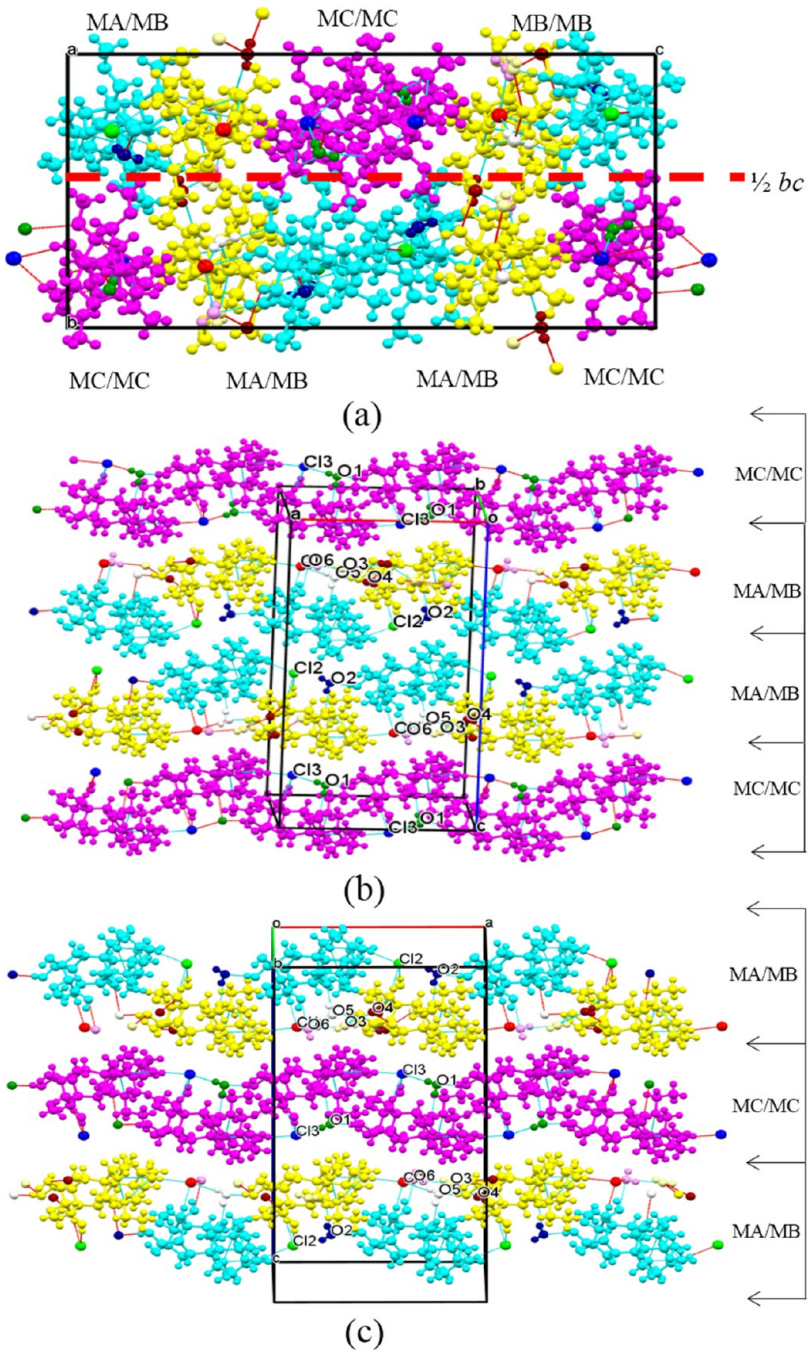

Figure 5. Crystal with the molecular stacking of AHD, showing (a) the packing structure for the *bc* plane, (b) a fragment of the two-dimensional layer (MC/MC-MA/MB-MA/MB-MC/MC), along with the lower $\frac{1}{2}$ *bc* plane [below the red dashed line in (a)], and (c) another fragment of the two-dimensional layer (MA/MB- MC/MC-MA/MB), along with the upper $\frac{1}{2}$ *bc* plane [above the red dotted line in (a)].

(Figure S1b), and MC (Figure S1c) cations represent three conformers with significant conformational differences observed in torsion angles surrounding nitrogen atoms (Table 2). Detailed analysis reveals that MA exhibits apparent dissimilarity from MB or MC, while MB and MC adopt nearly identical conformations. Furthermore, a comparison is made between the three aconine cations in AHD and those in AHM[22] through overlapping central frameworks (Figure 3). It is observed that the MA cation in AHD crystal closely resembles the M1 cation in AHM crystal (Figure 3a and Table 2), while the MB and MC cations in AHD exhibit almost identical conformations to the M2 and M3 cations, respectively, in AHM (Figure 3b and Table 2). Hence, it can be inferred that both AHD and AHM possess identical aconine cations within their respective crystal structures.

In this case of AHD, water molecules serve as donors and establish O−H···Cl^- hydrogen bonds with chloride anions, resulting in water−chloride interactions (Figures 2 and 3). Consequently, the Cl anions do not participate in the formation of intermolecular N^+−H···Cl^- hydrogen bonds in MA, MB, and MC cations, which is consistent with previous findings for AHM.[22] Conversely, in another instance of albendazole hydrochloride[33] without water molecules present in its crystal structure, the Cl anions are involved in the

https://doi.org/10.1021/acsomega.3c09696
ACS Omega 2024, 9, 11925−11941

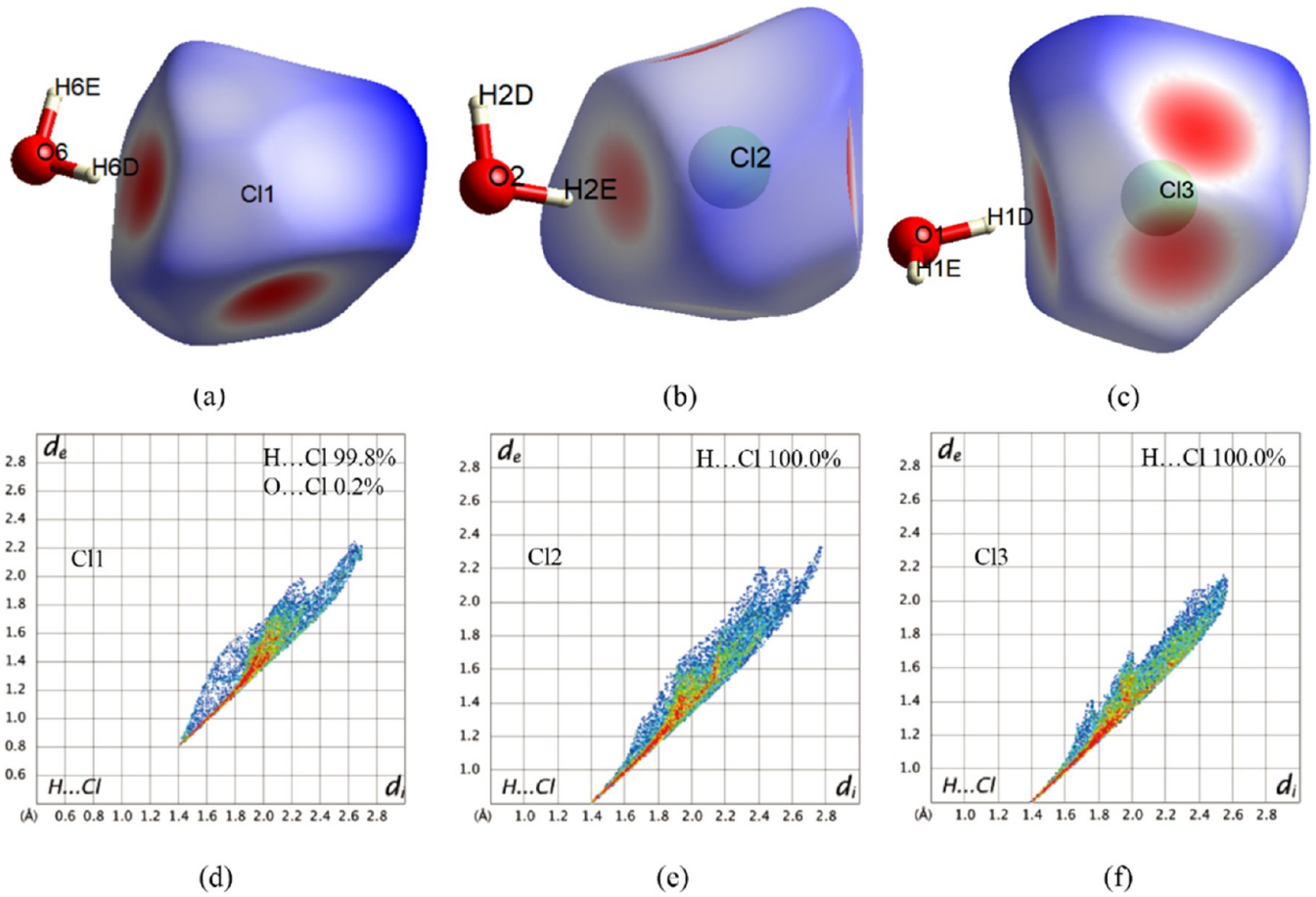

Figure 6. Hirshfeld surface (a–c) and fingerprint plot (d–f) for three Cl anions: (a, d) Cl1 anion; (b, e) Cl2 anion; (c, f) Cl3 anion.

formation of intermolecular $N^+-H\cdots Cl^-$ charge-assisted hydrogen bonds.

The aconine cation structure in AHD is superimposed onto that of lappaconitine, a nonaddictive analgesic used in China for various psychological and chronic pain conditions.[34] It has been found that the central framework of the aconine cation is identical to that of the lappaconitine cation in lappaconitine hydrobromide monohydrate (CCDC accession 241693). This similarity is also evident in neoline (CCDC accession 828610), which belongs to an active ingredient of the aconite family and exhibits ameliorative effects on mechanical hyperalgesia in diabetic mice.[35,36] Based on the structure–activity relationship, this aforementioned identical central framework confirms that AHD is likely to demonstrate similar pharmacological effects as lappaconitine[34] and neoline.[36] Indeed, experimental studies have validated the comparable analgesic effects of AHD and lappaconitine hydrobromide, although the corresponding data are not presented in this context.

3.2. Supramolecular Architecture. The hydrogen bonding geometry of AHD is summarized in Table 3, while the supramolecular architectures featuring key hydrogen bonds in the AHD crystal are depicted in Figure 4. The Cl1 and Cl2 anions and H_2O2 water molecule serve as pivotal connecting hubs, engaging in interactions with both MA and MB cations (Figure 4 and Table 3), thereby establishing three-dimensional hydrogen bonding networks that contribute to the supramolecular architecture of MA to MB (MA/MB) (Figure 4a). Likewise, the Cl3 anion and H_2O1 water molecule act as connecting hubs through their interactions with MC cations, resulting in three-dimensional hydrogen bonding networks that contribute to the supramolecular architecture of MC to MC (MC/MC) (Figure 4b). Comparable supramolecular architectures can be observed in the crystal structure of AHM.[22]

The hydroxyl group H8B–O8B serves as a bridge,[37] connecting Cl1 anion and H_2O5 water with three waters (H_2O4, H_2O3, and H_2O6) to form a one-dimensional hydrogen bonding chain (Figure 4c and Table 3). This chain establishes interactions among supramolecular architectures of MA/MB. The hydrogen bonding interactions O6–H6*D*···Cl1, O5–H5*D*···Cl1^{vi}, O6–H6*E*···O3, O3–H3*B*···O9*B*^{i} and O9*B*–H9*B*···O5 contribute to the formation of cyclic motif of $S(1)$; the hydrogen bonding interactions O3–H3*B*···O9*B*^{i}, O3–H3*A*···O4^{v} and O4–H4*D*···O5*B*^{viii} contribute to the formation of cyclic motif of $S(2)$; the hydrogen bonding interactions O8*B*–H8*B*···O5 and O9*B*–H9*B*···O5 contribute to the formation of cyclic motif of $S(3)$. Notably, this type of one-dimensional hydrogen bonding chain is absent in the AHM crystal structure.[22] In addition, the O5B atom in the MB cation accepts an H21F atom in the MC cation (Figure S2 and Table 3), forming an intermolecular C21*C*–H21*F*···O5*B* hydrogen bond that facilitates interactions between supramolecular architectures of MA/MB (Figure 4a) and MC/MC (Figure 4b).

3.3. Crystal Packing. The crystal packing of AHD is illustrated in Figure 5, depicting the arrangement of the supramolecular architectures. The supramolecular architectures of MC/MC, MA/MB, MA/MB, and MC/MC are organized into sheets along with the lower $\frac{1}{2}$ *bc* plane (Figure

https://doi.org/10.1021/acsomega.3c09696
ACS Omega 2024, 9, 11925–11941

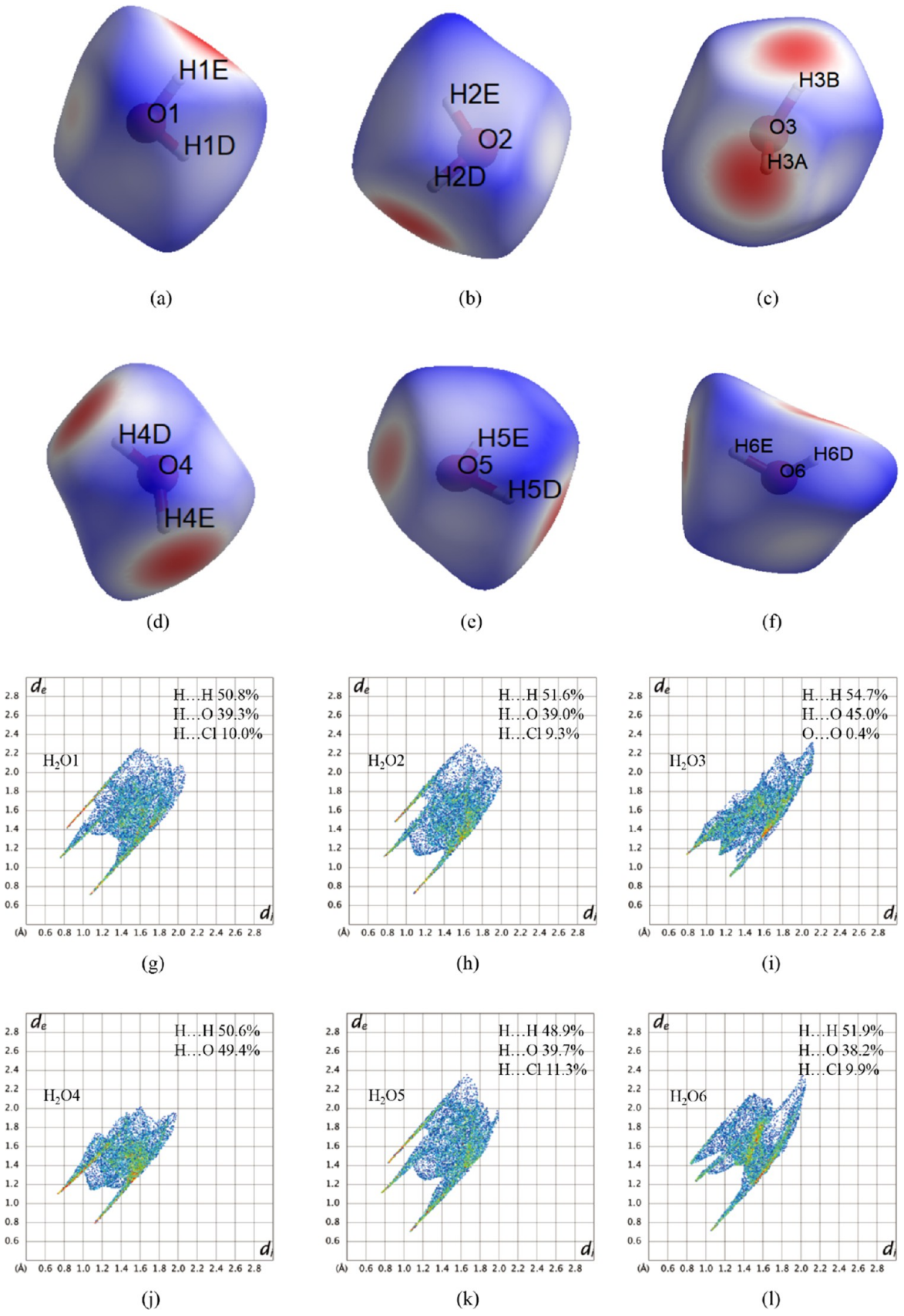

Figure 7. Hirshfeld surface (a–f) and fingerprint plot (g–l) for six water molecules: (a, g) H_2O1; (b, h) H_2O2; (c, i) H_2O3; (d, j) H_2O4; (e, k) H_2O5; (f, l) H_2O6.

https://doi.org/10.1021/acsomega.3c09696
ACS Omega 2024, 9, 11925−11941

5a), forming a fragment of the two-dimensional layer (Figure 5b). Similarly, along with the upper $\frac{1}{2}$ *bc* plane (Figure 5a), the supramolecular architectures of MA/MB, MC/MC, and MA/MB are arranged into sheets to generate another fragment of the two-dimensional layer (Figure 5c). These two fragments are then stacked in the crystallographic *b* direction to extend into a three-dimensional crystal structure. In contrast to the AHM crystal, where M3/M3, M1/M2, M1/M2, and M3/M3 supramolecular architectures[22] are aligned along the upper $\frac{1}{2}$ *bc* plane, while M1/M2, M3/M3, and M1/M2 supramolecular architectures[22] are arranged along the lower $\frac{1}{2}$ *bc* plane. In the AHD crystal, however, the stacking order of the crystal packing is completely reversed. This highlights once again the distinct disparities between the AHD and AHM crystals.

3.4. Hirshfeld Surface Analysis. The quantitative contributions[38] of various short contacts within the crystal structure were investigated using Hirshfeld surface analysis (Figures S3, 6, and 7) generated with CrystalExplorer (version 21.5).[39] Hirshfeld surface analysis (Figures S3a−h, 6a−c, and 7a−f) yields comprehensive three-dimensional maps, while its corresponding fingerprint analysis (Figures S3i−l, 6d−f, and 7g−l) presents concise two-dimensional plots.[40] The utilization of Hirshfeld surface analysis allows for more detailed insight into the key contacts in the supramolecular architectures of the AHD crystal.

In the Hirshfeld surfaces of the asymmetric unit of AHD crystal (Figure S3), the blue regions correspond to H···H contacts (Figure S3a,e) with distances longer than the van der Waals radii;[41] the red spots represent Cl^-···H/H···Cl^- (Figure S3b,f), O···H/H···O (Figure S3c,g), and O···O (Figure S3d,h) contacts with the distances shorter than the van der Waals radii; and the white areas indicate weaker contacts with the distances equal to the van der Waals radii. The size of the red spots reflects the intermolecular forces and provides insights into proportions of different forces between molecules or ions.[42] In terms of total surface, H···H (Figure S3i) contacts constitute a major proportion of relative interactions, accounting for approximately 71.8%; Cl^-···H/H···Cl^- (Figure S3g) and O···H/H···O (Figure S3k) contacts contribute 9.8 and 18.4%, respectively; besides the contacts involving H atoms, AHD also exhibits an O···O contact (Figure S3l) comprising only 0.1%. The Cl^-···H/H···Cl^- contacts externally manifested as two sharp spikes, while the O···H/H···O contacts internally displayed two sharp spikes as well, indicating high hydrogen bonding interactions[43] in the crystal packing. Considering the asymmetric unit of the AHD crystal, it is important to note that the red spots observed on Hirshfeld surfaces provide only a partial representation of the key intermolecular contacts. However, it should be emphasized that the current supramolecular architecture of the AHD crystal lacks information regarding the connecting hubs. Therefore, separate Hirshfeld surfaces will be generated for three chloride anions (Figure 6) and six water molecules (Figure 7) in order to further elucidate these pivotal intermolecular contacts.

The Hirshfeld surfaces (Figure 6) enclosing three Cl anions exhibit noticeable deformations due to the existence of short contacts (Figure 6a−c). The d_{norm} surface of the Cl1 anion (Figure 6a) distinctly displays regions with red spots, which correspond to the short contacts between the Cl1 anion and MA and MB cations, as well as H_2O5 and H_2O6 water molecules (Figure 4a), for the Cl2 anion (Figure 6b), which participates in the short contacts with MA and MB cations alongside the H_2O2 water molecule (Figure 4a), and for the Cl3 anion (Figure 6c), which is involved in the short contacts with MC cations together with the H_2O1 water molecule (Figure 4b). Consequently, distinctive feather-like patterns are discernible on fingerprint plots (Figure 6d−f). The Cl1 anion engages in both Cl^-···H/H···Cl^- and Cl^-···O/O···Cl^- contacts, collectively accounting for 100% of the surface (Figure 6a). In contrast, the Cl2 and Cl3 anions only participate in the Cl^-···H/H···Cl^- contact (Figure 6b,c), each contributing equally at a rate of 100%. Additionally, the contribution of the $Cl1^-$···O6/O6···$Cl1^-$ contact is small and negligible in the supramolecular architecture of MA/MB (Figure 4a). Undoubtedly, water−chloride interactions (H_2O5 and Cl1 anion; H_2O6 and Cl1 anion; H_2O2 and Cl2 anion; H_2O1 and Cl3 anion) play a significant role in stabilizing[16] the cohesive crystal lattice structure of AHD.

Likewise, the Hirshfeld surfaces of six water molecules exhibit anomalous behaviors, as anticipated due to the presence of short contacts (Figure 7a−f). Comparable observations have been reported in the case of 2,6-bis(1H-imidazol-2-yl) pyridine hydrochloride trihydrate.[44] The d_{norm} surface vividly depicts the regions where hydrogen bonding interactions involving the O and H atoms occur, which are visually emphasized by red spots. The participation of all water molecules in these H···O contacts can be classified into three distinct groups: the first group encompasses interactions between water molecules and cations (H_2O1 and MC; H_2O2 and MA; H_2O2 and MB; H_2O5 and MA; H_2O5 and MB); the second group comprises interactions between water molecules themselves as well as cation (H_2O4 and H_2O3; H_2O4 and MB); and the third group solely involves interactions between water molecules themselves (H_2O3 and H_2O4; H_2O3 and H_2O6). These specific types of hydrogen bonding interactions contribute to the Hirshfeld surfaces within a range of 38.2−49.4% (Figure 7g−l). Among six water molecules, H_2O1, H_2O2, and H_2O5 also engage in the H···Cl^- contacts with contributions ranging from 9.3 to 11.3% (Figure 7g,h,k). The involvement of H_2O3 in an O···O contact is negligible (Figure 7i) due to the absence of BCP. Clearly, water−water interactions play a crucial in shaping the crystal structure stability[17] of AHD; however, their precise influence remains yet unknown.

In this context, the correlation between Hirshfeld surface analysis and topological analysis may be limited due to their reliance on different partitioning schemes.[45] Specifically, Hirshfeld surface analysis is conducted using the spherical atom model, whereas Bader's Quantum Theory of Atoms in Molecules (QTAIM)[46] utilizes an aspherical multipolar model. A study has highlighted the discrepancies between these two approaches.[47] The subsequent section will delve into a comprehensive examination of short contacts, employing Bader's QTAIM approach to derive their topological properties for both quantitative and qualitative analyses.

3.5. H···O and H···Cl^- Contacts. Due to the limited resolution ($\sin\theta/\lambda$ around 0.625 $Å^{-1}$) of our diffraction experiment, multipole refinement was not feasible. Therefore, we employed the electron transfer-based MoPro-ELMAM2[30] model to gain insights into the electron density, strength, and nature of short contacts.[48] Furthermore, several studies[30,49] have confirmed that both multipole refinement and MoPro-ELMAM2 models exhibit a consistent trend in the topological

https://doi.org/10.1021/acsomega.3c09696
ACS Omega 2024, 9, 11925−11941

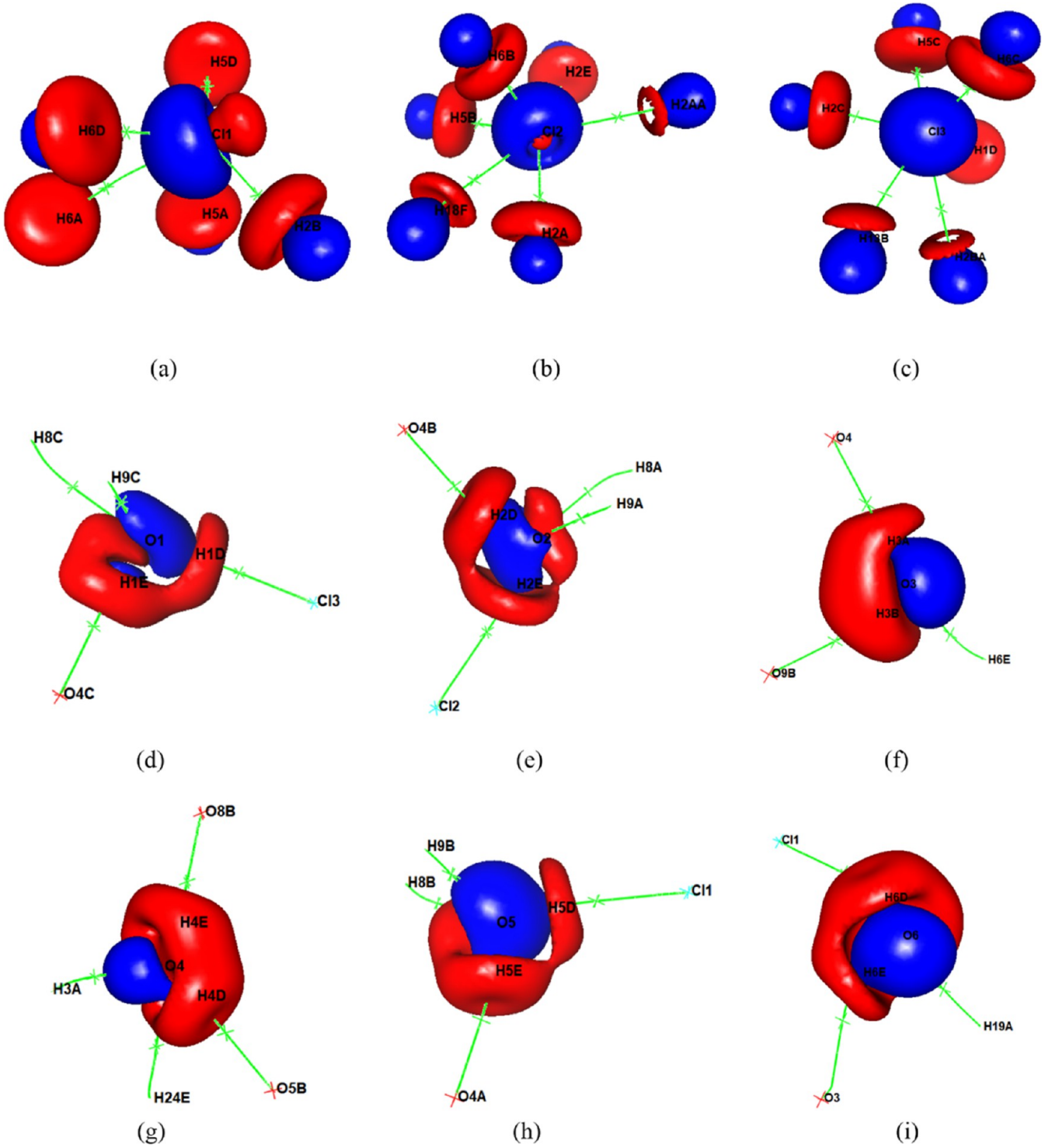

Figure 8. Three-dimensional plots for short contacts with Cl anions (a−c: Cl1 to Cl3) and water molecules (d−i: H_2O1 to H_2O6) from the Mopro-ELMAM2 model. Blue area indicates positive iso-surfaces, and the red area indicates negative iso-surfaces. Blue line indicates the key BCP paths around Cl anions and O atoms. Green cross indicates the key BCPs; red cross indicates O atoms; and cyan cross indicates Cl anions. The positive and negative iso-surfaces are drawn at intervals of 0.05 e $Å^{-3}$. For symmetry codes, see Table 3.

values at the BCPs and demonstrate excellent quantitative and qualitative agreement. In this study, our primary focus lies in investigating hydrogen bonding interactions involving the H···O and H···Cl^- contacts. Currently, direct analysis of electron density is utilized as a prominent method for obtaining valuable information regarding short contacts.[50] Detailed information on the topological analysis can be found in Tables S1 and S2.

According to the theory of atoms in molecules,[51] the presence of a critical point along the H···O path classifies it as a hydrogen bond.[52] Likewise, this theory also applies to identify other short contacts such as H···Cl^-. The investigation of (3, −1) BCPs within the asymmetric unit (Table S1) has revealed

https://doi.org/10.1021/acsomega.3c09696
ACS Omega 2024, 9, 11925−11941

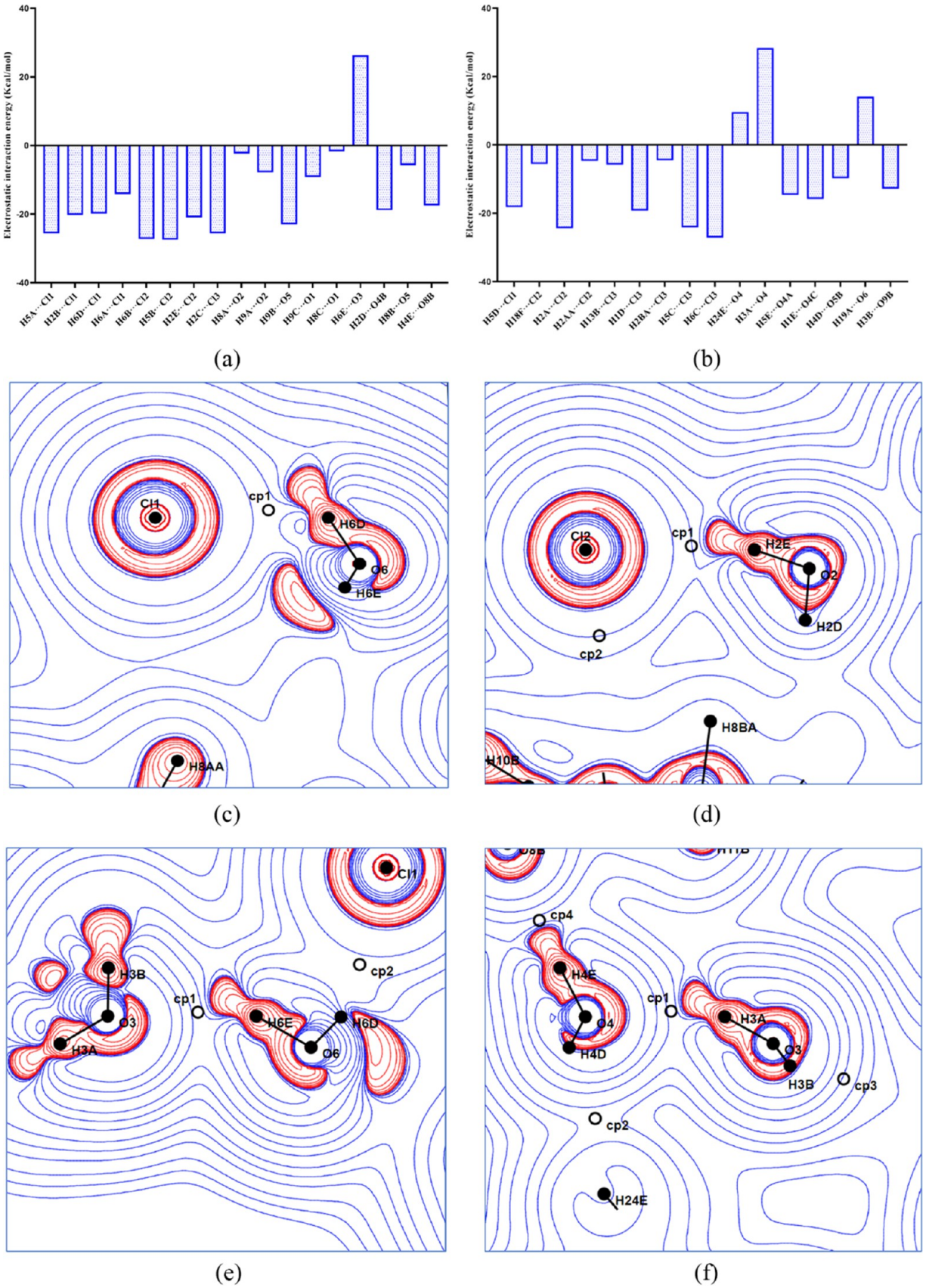

Figure 9. Bar plots of electrostatic interaction energy for short contacts with Cl anions and water molecules from the Mopro-ELMAM2 model for AHD within (a) or without (b) the asymmetric unit. Laplacian maps for H6D···$Cl1^-$ (c), H2E···$Cl2^-$ (d), H6E···O3 (e), and H3A···O4 (f) contacts in AHD. Contours are drawn at logarithmic intervals in $\nabla^2\rho(_{BCP})$, e $Å^{-5}$. Blue lines indicate positive contours, and red lines indicate negative contours. For symmetry codes, see Table 3.

https://doi.org/10.1021/acsomega.3c09696
ACS Omega 2024, 9, 11925−11941

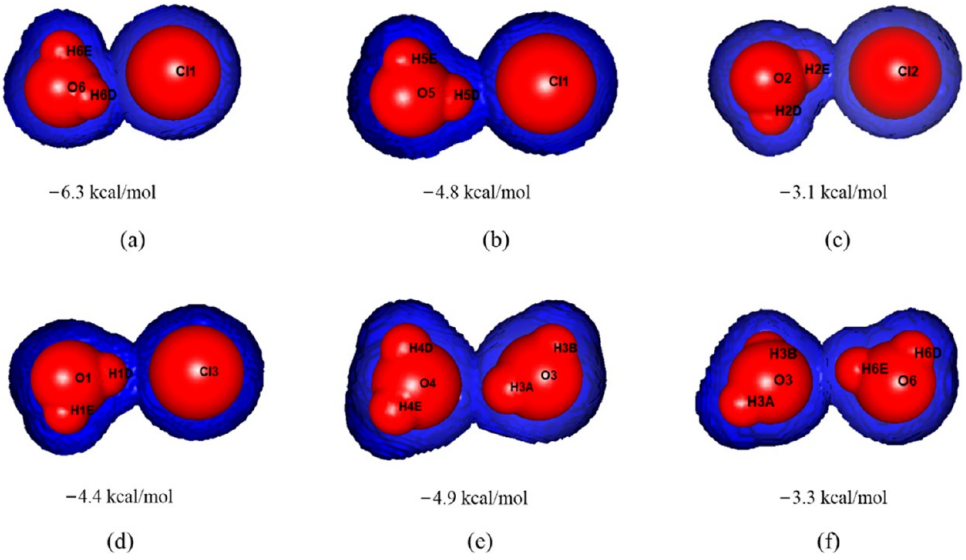

Figure 10. Electrostatic interaction energies for water−chloride (a−d) and water−water (e, f) interactions from the Mopro-ELMAM2 model.

a total of 17 hydrogen bonds. Moreover, upon examination of the (3, −1) BCPs without considering the asymmetric unit (Table S2), it has been suggested that there exist 16 hydrogen bonds. Analysis of Tables S1 and S2 reveals that positive contributions dominate in the H···O and H···Cl^- contacts involving chloride anion and water molecule for the AHD crystal with $\nabla^2\rho(BCP) > 0$.

The stabilization of the crystal structure is critically influenced by three Cl anions (Figure 8a−c, Tables S1 and S2), which act as acceptors and engage in multiple strong H···Cl^- contacts (Figure 4). The electron densities of these contacts range from 0.023 to 0.198 e $Å^{-3}$. These contacts exhibit Laplacian values within the range of 0.43 to 1.29 e $Å^{-5}$, indicating their distinctive closed-shell nature. The electrostatic energy between donor and acceptor ranges from 0.2 to 8.8 kcal/mol (Figure 9), suggesting that these attractive H···Cl^- and O··· Cl^- contacts play a significant role in the supramolecular architectures of MA/MB or MC/MC (Figure 4). However, each Cl anion plays a distinct role in the crystal lattice. First, the Cl1 anion acts as an acceptor in five H···Cl^- contacts (Tables S1, S2 and Figures 8a, 9a,b), with bond lengths ranging from 2.215 to 3.262 Å. The iso-surface at the Cl1 anion displays a red-to-blue area ratio of 0.24, while the total electrostatic energies between donor and acceptor are −19.9 kcal/mol. Second, the Cl2 anion functions as an acceptor in six H···Cl^- contacts (Tables S1, S2, and Figures 8b, 9a,b), with bond lengths ranging from 2.203 to 2.920 Å, a red-to-blue area ratio of iso-surface at Cl2 anion being 0.0033, and a total electrostatic energy of −24.1 kcal/mol. Finally, the Cl3 anion serves as an acceptor in six H···Cl^- contacts (Tables S1, S2 and Figures 8c, 9a,b) with bond lengths ranging from 2.198 to 2.880 Å. The iso-surface at the Cl3 anion has a red-to-blue area ratio of 0.0012, and the total electrostatic energies are −25.1 kcal/mol. Given all H···Cl^- contacts involved in stabilizing the supramolecular architectures of AHD, the H2C···Cl3 contact (Figure 9a) between Cl3 and MC cation exhibits a remarkably strong attractive electrostatic energy of −7.1 kcal/mol. Similarly, the H6D···Cl1 contact (Figure 9a,c) between H_2O6 water and Cl1 anion exhibits an attractive electrostatic energy of −4.1 kcal/mol, while the H2E···Cl2 contact (Figure 9a,d) between H_2O2 water and Cl2 anion displays an attractive electrostatic energy of −2.7 kcal/mol. Taken collectively, among these three studied Cl anions, both Cl2 and Cl3 anions exhibit comparable strengths; however, it is observed that the attractive force exhibited by the Cl1 anion is relatively weaker. Additionally, H···Cl^- contacts resulting from the interactions between chloride anions and cations show significantly greater strength compared to those formed between water molecules and chloride anions.

Water molecules not only play an essential role in the recognition between biomolecules[53] but also act as pivotal connectors, facilitating the assembly of diverse molecules or ions to build the crystal.[45] In addition to the H···Cl^- contacts that interact with water molecules, numerous H···O contacts are observed in the surrounding water molecules (Figure 4). These H···O contacts exhibit separations ranging from 1.784 to 2.707 Å, with $\rho BCP(r)$ values varying within the reported range of 0.029−0.292 e $Å^{-3}$, consistent with previous literature findings.[45] Their Laplacian values range from 0.344 to 1.485 e $Å^{-5}$, indicating that a closed-shell nature is present in these interactions. The electrostatic energy between donor and acceptor ranges from −0.4 to −8.8 kcal/mol (Figure 9a,b), suggesting all H···O contacts display attractive forces (Figures 4 and 5). Among these H···O contacts, the H9B···O5 contact (Figure 9a) between H_2O5 and the MB cation exhibits a remarkably strong attractive electrostatic energy of −8.8 kcal/mol. Similarly, the H6E···O3 contact (Figure 9a,e) between H_2O6 and H_2O3 displays an attractive electrostatic energy of −2.3 kcal/mol, while the H3A···O4 contact (Figure 9b,f) between H_2O3 and H_2O4 demonstrates an attractive electrostatic energy of −3.5 kcal/mol. In general terms, the six water molecules can be categorized based on their total electrostatic energies. The first category consists of H_2O6 and H_2O3 water molecules (Figure 8f,g), which possess electrostatic energies of −6.8 and −6.7 kcal/mol, respectively. The second category includes H_2O1, H_2O2, H_2O5, and H_2O4 water molecules (Figure 8d,e,h,i) with electrostatic energies of −17.3, −15.5, −15.9, and −11.8 kcal/mol, respectively. Among these water molecules, the Cl3 anion significantly enhances the electrostatic energies of H_2O1 (Figure 8d) while the Cl2 anion clearly strengthens the electrostatic energies of H_2O2 (Figure 8e). Additionally, the presence of the Cl1 anion simultaneously

https://doi.org/10.1021/acsomega.3c09696
ACS Omega 2024, 9, 11925−11941

enhances the electrostatic energies of both H_2O5 (Figure 8h) and H_2O6 (Figure 8i).

A fundamental characteristic of water and chloride anion is their ability to form hydrogen bonds, which are strong interactions with other polar molecules and themselves. The stability of hydrogen bonds can range from −0.2 to −40 kcal/mol, depending on the specific O and Cl species involved as well as the geometry of the hydrogen bond.[54] Our findings clearly indicate that all H···O contacts play a crucial role in stabilizing the crystal structure of AHD. It is worth noting that H···O contacts between water molecules and cations exhibit significantly greater strength compared to those formed among water molecules. Additionally, each water molecule assumes a distinct function in facilitating the assembly of anions or cations for crystal formation.

3.6. Water−Chloride and Water−Water Interactions. Regarding the water−chloride interactions, the electrostatic energies range from −3.1 to −6.3 kcal/mol (Figure 10a−d). The interaction between H_2O6 and $Cl1^-$ (Figure 10a) demonstrates the highest level of attraction, followed by those between H_2O5 and $Cl1^-$ (Figure 10b), as well as those between H_2O1 and $Cl3^-$ (Figure 10d). Conversely, the interaction between H_2O2 and $Cl2^-$ (Figure 10c) shows a comparatively lower level of attraction within this system. Remarkably, our computational results align with previous experimental investigations on water−chloride interactions.[16]

Meanwhile, in terms of the water−water interactions, an attractive electrostatic energy of −4.9 kcal/mol exists between H_2O4 and H_2O3 water molecules (Figure 10e), while there is also an attractive electrostatic energy of −3.3 kcal/mol observed between H_2O3 and H_2O6 water molecules (Figure 10f). These attractive energies for water−water interactions fall within the range (−0.3 to −6.0 kcal/mol)[17] calculated for crystal structures reported in the Cambridge Structural Database.

The stability of AHD in its solid-state form is supported by electrostatic energy calculations, which demonstrate the electrostatic attraction of both interactions between water and chloride anions as well as interactions among water molecules. This theoretical basis will contribute to future investigations on AHD storage and safe processing.[3]

4. CONCLUSIONS

The present study focuses on the structural analysis of a new dihydrate form of aconine hydrochloride, which can serve as an alternative to the monohydrate form for enhancing the preparative technology of WuTou injection. Both AHD and AHM exhibit identical aconine cations within their crystal structures; however, significant differences exist between their respective crystal structures, primarily related to water molecules. In the AHD crystal, ideal displacement factors were employed during refinement to accurately determine the positions of water molecules, while in the AHM crystal, squeezed procedures were applied to remove several disordered water molecules.

Due to the involvement of multiple water molecules in the constitution of AHD crystal, the Cl anions do not participate in the formation of intermolecular N^+−H···Cl^- charge-assisted hydrogen bonds in MA, MB, and MC cations; instead, they contribute to fulfilling the strongest intramolecular N^+−H···O charge-assisted hydrogen bonds within the cations. Three Cl anions are involved in water−chloride interactions and stabilize the crystal structure through intermolecular H···Cl^- contacts. Similarly, three water molecules engage in water−water interactions and enhance the stability of the crystal structure by means of the intermolecular H···O contacts. Notably, the support of the literature adds value to the present work.

Taken with the existing evidence from this work, this study quantitatively evaluates the topological properties of H···Cl^- and O···Cl^- contacts as well as the electrostatic energies resulting from both water−chloride and water−water interactions. The future research focus will be directed toward investigating the stability properties of AHD to facilitate drug development.

■ ASSOCIATED CONTENT

Supporting Information

The Supporting Information is available free of charge at https://pubs.acs.org/doi/10.1021/acsomega.3c09696.

Displacement ellipsoid plots for each aconine cation; simplified view of the key hydrogen bonds occurring in the asymmetric unit of AHD; Hirshfeld surface and Fingerprint plot for the asymmetric unit of AHD; and topological features associated with and without the asymmetric unit (PDF)

Accession Codes

The supplementary crystallographic data (CCDC 2296364, 2296449, 2296450) for this paper can be obtained free of charge through the following methods: accessing www.ccdc.cam.ac.uk/data_request/cif, sending an email to data_request@ccdc.cam.ac.uk, or contacting The Cambridge Crystallographic Data Centre at 12 Union Road, Cambridge CB2 1EZ, UK; fax: + 44 1223 336033.

■ AUTHOR INFORMATION

Corresponding Author

Han-Qing Li − *State Clinical Trial Institution of New Drugs and Mongolian Medicine Laboratory, International Mongolian Hospital of Inner Mongolia, Hohhot, Inner Mongolia 010065, People's Republic of China*; orcid.org/0000-0002-8837-532X; Email: hqltcm@163.com

Authors

Jia-Yin Xu − *Mongolian Pharmaceutical Preparation Center, International Mongolian Hospital of Inner Mongolia, Hohhot, Inner Mongolia 010065, People's Republic of China*

Shan-Shan Wu − *State Clinical Trial Institution of New Drugs, International Mongolian Hospital of Inner Mongolia, Hohhot, Inner Mongolia 010065, People's Republic of China*

Liang Jin − *State Clinical Trial Institution of New Drugs, International Mongolian Hospital of Inner Mongolia, Hohhot, Inner Mongolia 010065, People's Republic of China*

Complete contact information is available at: https://pubs.acs.org/10.1021/acsomega.3c09696

Author Contributions

The manuscript was collaboratively written by all authors, and the final version has received approval from all of them.

Notes

The authors declare no competing financial interest.

■ ACKNOWLEDGMENTS

The authors express sincere gratitude for the support of this research from the scientific and technological project of Inner Mongolia Autonomous Region Health Commission

(202202054), the Natural Science Foundation of Inner Mongolia Autonomous Region (2021MS08100), the Mongolian medicine development/Mongolian medicine lab construction project in Mongolian medicine institute (2016YJS10), and the scientific and technological project of Inner Mongolia Autonomous Region (2013KJTXM).

REFERENCES

(1) Braun, D. E.; Lingireddy, S. R.; Beidelschies, M. D.; Guo, R.; Müller, P.; Price, S. L.; Reutzel-Edens, S. M. Unraveling Complexity in the Solid Form Screening of a Pharmaceutical Salt: Why so Many Forms? Why so Few? *Cryst. Growth Des.* **2017**, *17* (10), 5349−5365.
(2) Huang, D.; Yang, D.; Lv, Y.; Zhou, J.; Li, L.; Xu, J.; Yang, X.; Zhou, Z. Lattice water provides hydrogen atom donor to form hydrate: A case study of chlorbipram: m-hydroxybenzoic acid (1:1) cocrystal. *J. Mol. Struct.* **2022**, *1250*, No. 131891.
(3) Hespeler, D.; Pyo, S. M.; Müller, R. H. Dermal smartPearls - Optimized silica particles for commercial products & mechanistic considerations. *Int. J. Pharm.* **2020**, *574*, No. 118757. Wolbert, F.; Nikoleit, K.; Steinbrink, M.; Luebbert, C.; Sadowski, G. The Shelf Life of ASDs: 1. Measuring the Crystallization Kinetics at Humid Conditions. *Mol. Pharmaceutics* **2022**, *19* (7), 2483−2494. Okezue, M.; Bogdanowich-Knipp, S.; Smith, D.; Zeller, M.; Byrn, S.; Smith, P.; Purcell, D. K.; Clase, K. Salts and Polymorph Screens for Bedaquiline. *AAPS PharmSciTech* **2021**, *22* (7), No. 228.
(4) Rajput, L. Stable Crystalline Salts of Haloperidol: A Highly Water-Soluble Mesylate Salt. *Cryst. Growth Des.* **2014**, *14* (10), 5196−5205.
(5) Braun, D. E.; Gelbrich, T.; Kahlenberg, V.; Griesser, U. J. Insights into hydrate formation and stability of morphinanes from a combination of experimental and computational approaches. *Mol. Pharmaceutics* **2014**, *11* (9), 3145−3163.
(6) Posavec, L.; Nemec, V.; Stilinović, V.; Cinčić, D. Halogen and Hydrogen Bond Motifs in Ionic Cocrystals Derived from 3-Halopyridinium Halogenides and Perfluorinated Iodobenzenes. *Cryst. Growth Des.* **2021**, *21* (11), 6044−6050.
(7) Fotović, L.; Stilinović, V. Halogenide anions as halogen and hydrogen bond acceptors in iodopyridinium halogenides. *CrystEngComm* **2020**, *22* (23), 4039−4046.
(8) van Terwingen, S.; Brüx, D.; Wang, R.; Englert, U. Hydrogen-Bonded and Halogen-Bonded: Orthogonal Interactions for the Chloride Anion of a Pyrazolium Salt. *Molecules* **2021**, *26* (13), No. 3982, DOI: 10.3390/molecules26133982.
(9) Fotović, L.; Bedeković, N.; Stilinović, V. Isostructural Halogen Exchange and Halogen Bonds: The Case of N-(4-Halogenobenzyl)-3-halogenopyridinium Halogenides. *Cryst. Growth Des.* **2022**, *22* (2), 1333−1344.
(10) Hathwar, V. R.; Gonnade, R. G.; Munshi, P.; Bhadbhade, M. M.; Guru Row, T. N. Halogen Bonding in 2,5-Dichloro-1,4-benzoquinone: Insights from Experimental and Theoretical Charge Density Analysis. *Cryst. Growth Des.* **2011**, *11* (5), 1855−1862. Widner, D. L.; Knauf, Q. R.; Merucci, M. T.; Fritz, T. R.; Sauer, J. S.; Speetzen, E. D.; Bosch, E.; Bowling, N. P. Intramolecular Halogen Bonding Supported by an Aryldiyne Linker. *J. Org. Chem.* **2014**, *79* (13), 6269−6278.
(11) Turunen, L.; Erdélyi, M. Halogen bonds of halonium ions. *Chem. Soc. Rev.* **2020**, *49* (9), 2688−2700.
(12) Milovanović, M. R.; Živković, J. M.; Ninković, D. B.; Stanković, I. M.; Zarić, S. D. How flexible is the water molecule structure? Analysis of crystal structures and the potential energy surface. *Phys. Chem. Chem. Phys.* **2020**, *22* (7), 4138−4143. Jurczak, E.; Mazurek, A. H.; Szeleszczuk, Ł.; Pisklak, D. M.; Zielińska-Pisklak, M. Pharmaceutical Hydrates Analysis-Overview of Methods and Recent Advances. *Pharmaceutics* **2020**, *12* (10), No. 959, DOI: 10.3390/pharmaceutics12100959.
(13) Curnow, O. J.; Crittenden, D. L. Structures and Spectra of Halide Hydrate Clusters in the Solid State: A Link between the Gas Phase and Solution State. *ChemPlusChem* **2022**, *87* (2), No. e202100535.
(14) Hoque, M. N.; Basu, A.; Das, G. Cyclic Pentameric Puckered Hybrid Chloride−Water Cluster [Cl3(H2O)4]3− in the Hydrophobic Architecture. *Cryst. Growth Des.* **2012**, *12* (5), 2153−2157.
(15) Phan, C.; Shen, J.; Yu, K.; Liu, J.; Tang, G. Hydrogen Bonds, Topologies, Energy Frameworks and Solubilities of Five Sorafenib Salts. *Int. J. Mol. Sci.* **2021**, *22* (13), No. 6682, DOI: 10.3390/ijms22136682.
(16) Dey, B.; Choudhury, S. R.; Gamez, P.; Vargiu, A. V.; Robertazzi, A.; Chen, C. Y.; Lee, H. M.; Jana, A. D.; Mukhopadhyay, S. Water-chloride and water-bromide hydrogen-bonded networks: influence of the nature of the halide ions on the stability of the supramolecular assemblies. *J. Phys. Chem. A* **2009**, *113* (30), 8626−8634.
(17) Milovanović, M. R.; Stanković, I. M.; Živković, J. M.; Ninković, D. B.; Hall, M. B.; Zarić, S. D. Water: new aspect of hydrogen bonding in the solid state. *IUCrJ* **2022**, *9*, 639−647.
(18) Saha, S. Effect of Water on the Molecular Structure and Arrangement of Nitrile-Functionalized Ionic Liquids. *J. Phys. Chem. B* **2006**, *110* (6), 2777−2781. Kotov, N.; Šturcová, A.; Zhigunov, A.; Raus, V.; Dybal, J. Structural Transitions of 1-Butyl-3-methylimidazolium Chloride/Water Mixtures Studied by Raman and FTIR Spectroscopy and WAXS. *Cryst. Growth Des.* **2016**, *16* (4), 1958−1967.
(19) Wang, F. P.; Chen, Q. H.; Liu, X. Y. Diterpenoid alkaloids. *Nat. Prod. Rep.* **2010**, *27* (4), 529−570.
(20) Huan, X.; Song, X. Pharmacological experiment of Wutou injection. *Qilu Yaoshi.* **1988**, 33−34.
(21) Pharmacopoeia Committee of the People's Republic of China. *Chinese Pharmacopoeia*, China Medical Science Press, 2020.
(22) Li, H. Q.; Xu, J. Y.; Gao, Y. Y.; Jin, L.; Chen, J. M.; Chen, F. Z. Supramolecular structure, in vivo biological activities and molecular-docking-based potential cardiotoxic exploration of aconine hydrochloride monohydrate as a novel salt form. *Acta Crystallogr., Sect. B: Struct. Sci., Cryst. Eng. Mater.* **2020**, *76* (2), 208−224.
(23) Krause, L.; Herbst-Irmer, R.; Sheldrick, G. M.; Stalke, D. Comparison of silver and molybdenum microfocus X-ray sources for single-crystal structure determination. *J. Appl. Crystallogr.* **2015**, *48* (Pt 1), 3−10.
(24) Sheldrick, G. M. Crystal structure refinement with SHELXL. *Acta Crystallogr.* **2015**, *71*, 3−8, DOI: 10.1107/S2053229614024218.
(25) Rigaku, O. D., *CrysAlis PRO*, Rigaku Oxford Diffraction Ltd,Yarnton, Oxfordshire, England, 2015.
(26) Dolomanov, O. V.; Bourhis, L. J.; Gildea, R. J.; Howard, J. A. K.; Puschmann, H. OLEX2: a complete structure solution, refinement and analysis program. *J. Appl. Crystallogr.* **2009**, *42*, 339−341.
(27) Sheldrick, G. M. A short history of SHELX. *Acta Crystallogr., Sect. A: Found. Crystallogr.* **2008**, *64*, 112−122.
(28) Jelsch, C.; Guillot, B.; Lagoutte, A.; Lecomte, C. Advances in protein and small-molecule charge-density refinement methods using MoPro. *J. Appl. Crystallogr.* **2005**, *38* (1), 38−54.
(29) Hansen, N. K.; Coppens, P. Testing aspherical atom refinements on small-molecule data sets. *Acta Crystallogr., Sect. A* **1978**, *34* (6), 909−921.
(30) Domagała, S.; Fournier, B.; Liebschner, D.; Guillot, B.; Jelsch, C. An improved experimental databank of transferable multipolar atom models–ELMAM2. Construction details and applications. *Acta Crystallogr., Sect. A: Found. Crystallogr.* **2012**, *68* (Pt 3), 337−351.
(31) Spek, A. L. PLATON SQUEEZE: a tool for the calculation of the disordered solvent contribution to the calculated structure factors. *Acta Crystallogr., Sect. C: Struct. Chem.* **2015**, *71*, 9−18, DOI: 10.1107/s2053229614024929.
(32) Rajput, L.; Banik, M.; Yarava, J. R.; Joseph, S.; Pandey, M. K.; Nishiyama, Y.; Desiraju, G. R. Exploring the salt-cocrystal continuum with solid-state NMR using natural-abundance samples: implications for crystal engineering. *IUCrJ* **2017**, *4* (Pt 4), 466−475.
(33) Bongioanni, A.; Bueno, M. S.; Abraham-Miranda, J.; Chattah, A. K.; Ayala, A. P.; Longhi, M. R.; Garnero, C. Investigating a Soluble

https://doi.org/10.1021/acsomega.3c09696
ACS Omega 2024, 9, 11925−11941

Pharmaceutical Salt: Albendazole Hydrochloride. *Cryst. Growth Des.* **2019**, *19* (8), 4538−4545.
(34) Li, Y.; Shang, Y.; Li, X.; Zhang, Y.; Xie, J.; Chen, L.; Gao, F.; Zhou, X. L. Design, synthesis, and biological evaluation of low-toxic lappaconitine derivatives as potential analgesics. *Eur. J. Med. Chem.* **2022**, *243*, No. 114776.
(35) Li, H.; Xu, J.; Zhang, X.; Liu, C.; Chen, N.; Naruo, A.; Qin, Z.; Ao, M. New napelline-type diterpenoid alkaloids from Aconiti kusnezoffii roots: Structure elucidation, plausible biogenetic pathway and biological activities. *Phytochem. Lett.* **2021**, *43*, 53−59.
(36) Nakatani, Y.; Negoro, K.; Yamauchi, M.; Katasho, M.; Ishikura, K. I.; Iwaki, A.; Tsukada, K.; Yamaguchi, M.; Uehara, A.; Yoshida, M.; et al. Neoline, an active ingredient of the processed aconite root in Goshajinkigan formulation, targets Nav1.7 to ameliorate mechanical hyperalgesia in diabetic mice. *J. Ethnopharmacol.* **2020**, *259*, No. 112963.
(37) Zhou, X.; Hu, X.; Wu, S.; Ye, J.; Sun, M.; Gu, J.; Zhu, J.; Zhang, Z. Structures and physicochemical properties of vortioxetine salts. *Acta Crystallogr., Sect. B: Struct. Sci., Cryst. Eng. Mater.* **2016**, *72*, 723−732. Smith, G.; Wermuth, U. D. The three-dimensional hydrogen-bonded structures in the ammonium and sodium salt hydrates of 4-aminophenylarsonic acid. *Acta Crystallogr., Sect. C: Struct. Chem.* **2014**, *70*, 738−741.
(38) McKinnon, J. J.; Jayatilaka, D.; Spackman, M. A. Towards quantitative analysis of intermolecular interactions with Hirshfeld surfaces. *Chem. Commun.* **2007**, No. 37, 3814−3816.
(39) Spackman, P. R.; Turner, M. J.; McKinnon, J. J.; Wolff, S. K.; Grimwood, D. J.; Jayatilaka, D.; Spackman, M. A. CrystalExplorer: a program for Hirshfeld surface analysis, visualization and quantitative analysis of molecular crystals. *J. Appl. Crystallogr.* **2021**, *54*, 1006−1011.
(40) Wzgarda-Raj, K.; Rybarczyk-Pirek, A. J.; Wojtulewski, S.; Palusiak, M. N-Oxide-N-oxide interactions and Cl···Cl halogen bonds in pentachloropyridine N-oxide: the many-body approach to interactions in the crystal state. *Acta Crystallogr.* **2018**, *74*, 113−119, DOI: 10.1107/s2053229617017922.
(41) Masoudiasl, A.; Montazerozohori, M.; Joohari, S.; Taghizadeh, L.; Mahmoudi, G.; Assoud, A. Structural investigation of a new cadmium coordination compound prepared by sonochemical process: Crystal structure, Hirshfeld surface, thermal, TD-DFT and NBO analyses. *Ultrason. Sonochem.* **2019**, *52*, 244−256.
(42) Han, Y.; Fu, Q.; Zhang, P.; Guan, H.; Guo, F. Acid-ammonium heterodimer and N(ammonium)-H···N(pyridine) synthon preference in three salts of nicotinic acid with (1R,2R)-1,2-diphenylethylenediamine. *Acta Crystallogr.* **2019**, *B75* (2), 219−226.
(43) Toularoud, M. E.; Pourayoubi, M.; Dušek, M.; Eigner, V.; Damodaran, K. Chiral one-dimensional hydrogen-bonded architectures constructed from single-enantiomer phosphoric triamides. *Acta Crystallogr.* **2018**, *74*, 608−617, DOI: 10.1107/S2053229618004734.
(44) Guerra, R. B.; Huamaní, L. S. C.; Tenorio, J. C.; Guimarães, W. M.; Bonacin, J. A.; Barboza Formiga, A. L. Analysis of solvent-accessible voids and proton-coupled electron transfer of 2,6-bis(1H-imidazol-2-yl)pyridine and its hydrochloride. *Acta Crystallogr.* **2019**, *75*, 1359−1371.
(45) Domagała, S.; Munshi, P.; Ahmed, M.; Guillot, B.; Jelsch, C. Structural analysis and multipole modelling of quercetin monohydrate–a quantitative and comparative study. *Acta Crystallogr.* **2011**, *67* (Pt 1), 63−78.
(46) Bader, R. F. W. A Bond Path: A Universal Indicator of Bonded Interactions. *J. Phys. Chem. A* **1998**, *102* (37), 7314−7323.
(47) Spackman, M. A.; Jayatilaka, D. Hirshfeld surface analysis. *CrystEngComm* **2009**, *11* (1), 19−32.
(48) Wang, A.; Wang, R.; Kalf, I.; Dreier, A.; Lehmann, C. W.; Englert, U. Charge-Assisted Halogen Bonds in Halogen-Substituted Pyridinium Salts: Experimental Electron Density. *Cryst. Growth Des.* **2017**, *17* (5), 2357−2364.
(49) Bisseyou, Y. B. M.; Bouhmaida, N.; Guillot, B.; Lecomte, C.; Lugan, N.; Ghermani, N.; Jelsch, C. Experimental and database-transferred electron-density analysis and evaluation of electrostatic forces in coumarin-102 dye. *Acta Crystallogr., Sect. B: Struct. Sci.* **2012**, *68*, 646−660, DOI: 10.1107/S0108768112042826. Saifina, A. F.; Kartashov, S. V.; Saifina, L. F.; Fayzullin, R. R. Applicability of transferable multipole pseudo-atoms for restoring inner-crystal electronic force density fields. Chemical bonding and binding features in the crystal and dimer of 1,3-bis(2-hydroxyethyl)-6-methyluracil. *IUCrJ* **2023**, *10*, 584−602. Jelsch, C.; Bisseyou, Y. B. M. Deciphering the driving forces in crystal packing by analysis of electrostatic energies and contact enrichment ratios. *IUCrJ* **2023**, *10*, 557−567, DOI: 10.1107/S2052252523005675.
(50) Guillén, M.; Mora, A. J.; Belandria, L. M.; Seijas, L. E.; Ramírez, J. W.; Burgos, J. L.; Rincón, L.; Delgado, G. E. Two conformational polymorphs of 4-methylhippuric acid. *Acta Crystallogr., Sect. B: Struct. Sci., Cryst. Eng. Mater.* **2020**, *76* (Pt 6), 1077−1091, DOI: 10.1107/S2052520620013773.
(51) Bader, R. F. W. Atoms in molecules:*A Quantum Theory* 1990.
(52) Fournier, B.; Bendeif, E.-E.; Guillot, B.; Podjarny, A.; Lecomte, C.; Jelsch, C. Charge Density and Electrostatic Interactions of Fidarestat, an Inhibitor of Human Aldose Reductase. *J. Am. Chem. Soc.* **2009**, *131* (31), 10929−10941.
(53) Howard, E. I.; Guillot, B.; Blakeley, M. P.; Haertlein, M.; Moulin, M.; Mitschler, A.; Cousido-Siah, A.; Fadel, F.; Valsecchi, W. M.; Tomizaki, T.; et al. High-resolution neutron and X-ray diffraction room-temperature studies of an H-FABP-oleic acid complex: study of the internal water cluster and ligand binding by a transferred multipolar electron-density distribution. *IUCrJ* **2016**, *3* (Pt2), 115−126.
(54) Steiner, T. The hydrogen bond in the solid state. *Angew. Chem., Int. Ed.* **2002**, *41* (1), 49−76, DOI: 10.1002/1521-3773(20020104)41:13.0.CO;2-U.

https://doi.org/10.1021/acsomega.3c09696
ACS Omega 2024, 9, 11925−11941